TECHNICAL REVIEW

Transmission Loss Measurements in a Standing Wave Tube

No.1 2007

Brüel & Kjær

Previously issued numbers of Brüel & Kjær Technical Review

1 – 2006 Dyn-X Technology: 160 dB in One Input Range
Order Tracking in Vibro-acoustic Measurements: A Novel Approach Eliminating the Tacho Probe
Comparison of Acoustic Holography Methods for Surface Velocity Determination on a Vibrating Panel

1 – 2005 Acoustical Solutions in the Design of a Measurement Microphone for Surface Mounting
Combined NAH and Beamforming Using the Same Array
Patch Near-field Acoustical Holography Using a New Statistically Optimal Method

1 – 2004 Beamforming

1 – 2002 A New Design Principle for Triaxial Piezoelectric Accelerometers
Use of FE Models in the Optimisation of Accelerometer Designs
System for Measurement of Microphone Distortion and Linearity from Medium to Very High Levels

1 – 2001 The Influence of Environmental Conditions on the Pressure Sensitivity of Measurement Microphones
Reduction of Heat Conduction Error in Microphone Pressure Reciprocity Calibration
Frequency Response for Measurement Microphones – a Question of Confidence
Measurement of Microphone Random-incidence and Pressure-field Responses and Determination of their Uncertainties

1 – 2000 Non-stationary STSF

1 – 1999 Characteristics of the vold-Kalman Order Tracking Filter

1 – 1998 Danish Primary Laboratory of Acoustics (DPLA) as Part of the National Metrology Organisation
Pressure Reciprocity Calibration – Instrumentation, Results and Uncertainty
MP.EXE, a Calculation Program for Pressure Reciprocity Calibration of Microphones

1 – 1997 A New Design Principle for Triaxial Piezoelectric Accelerometers
A Simple QC Test for Knock Sensors
Torsional Operational Deflection Shapes (TODS) Measurements

2 – 1996 Non-stationary Signal Analysis using Wavelet Transform, Short-time Fourier Transform and Wigner-Ville Distribution

1 – 1996 Calibration Uncertainties & Distortion of Microphones.
Wide Band Intensity Probe. Accelerometer Mounted Resonance Test

2 – 1995 Order Tracking Analysis

1 – 1995 Use of Spatial Transformation of Sound Fields (STSF) Techniques in the Automative Industry

(Continued on cover page 3)

Technical Review

No. 1 – 2007

Contents

TRADEMARKS

Thinsulate is a trademark of 3M Corporation in the United States and/or other countries
PULSE is a trademark of Brüel & Kjær Sound and Vibration Measurement A/S

Editor: Harry K. Zaveri

Measurement of Normal Incidence Transmission Loss and Other Acoustical Properties of Materials Placed in a Standing Wave Tube

J. Stuart Bolton and Taewook Yoo
Ray W. Herrick Laboratories
School of Mechanicl Engineering
Purdue University
West Lafayette, Indiana, USA

Oliviero Olivieri
Brüel & Kjær
Sound & Vibration Measurement A/S
Nærum, Denmark

Abstract
A method for measuring the normal incidence transmission loss and related acoustical properties of a sample placed in a four-microphone standing wave tube is described here. A conventional, two-microphone impedance tube, Brüel & Kjær's Type 4206, was connected to a sample holder downstream of the first microphone pair and a section downstream of the sample holder that accommodates a second pair of microphones. Sound pressure measurements on both sides of a piece of material placed in the sample holder for two different tube termination conditions (open and approximately anechoic) are typically used to estimate the two-by-two transfer matrix that characterises the sample. When the sample under test is symmetric front-to-back, a single measurement with one tube termination condition is sufficient to determine the transfer matrix elements. The transfer matrix elements can be used to calculate the transmission loss of the sample as well as a variety of other acoustical properties. The procedure is demonstrated here through measurement of a complete set of the acoustical properties of a fibrous material.

Résumé
Est décrite ci-après une méthode pour mesurer sous incidence normale la perte par transmission et autres propriétés acoustiques d'un échantillon de matériau placé dans un tube à ondes stationnaires à quatre microphones : un tube de Kundt conventionnel, le Tube de mesure de l'impédance à deux microphones Type 4206 de Brüel & Kjær, est connecté à un support d'échantillon de matériau placé en aval de

la première paire de microphones ; la deuxième paire de microphones est placée au niveau de la section située en aval du support. Des mesures de pression acoustique en amont et en aval de l'échantillon, pour deux modes de terminaison différents du tube (terminaison ouverte et approximativement anéchoïque), sont utilisées pour l'estimation de la matrice de transfert deux à deux caractérisant l'échantillon. Quand l'échantillon testé présente une symétrie avant/arrière, une seule mesure avec un seul mode de terminaison du tube suffit à déterminer les éléments de la matrice de transfert. Ces éléments sont utilisables pour le calcul de la perte de transmission sonore et de plusieurs autres propriétés acoustiques du matériau. La procédure est ici présentée et démontrée dans le cadre du mesurage des propriétés acoustiques d'un matériau fibreux.

Zusammenfassung

Es wird eine Methode zur Messung des Übertragungsverlustes bei senkrechtem Schalleinfall und von weiteren akustischen Eigenschaften einer Materialprobe in einem Vier-Mikrofon-Impedanzrohr mit stehenden Wellen beschrieben. Ein herkömmliches Impedanzrohr mit zwei Mikrofonen, Typ 4206 von Brüel & Kjær, wurde mit einem Probenhalter hinter dem ersten Mikrofonpaar und einem Abschnitt hinter dem Probehalter verbunden, der ein zweites Mikrofonpaar enthält. In der Regel werden Schalldruckmessungen auf beiden Seiten des im Probenhalter angebrachten Materials für zwei verschiedene akustische Rohrabschlüsse (offen und annähernd reflexionsfrei) ausgeführt, um die 2×2-Übertragungsmatrix der Probencharakteristik zu bestimmen. Wenn die Materialprobe im Längsschnitt symmetrisch ist, reicht eine einzige Messung mit nur einem Rohrabschluss aus, um die Elemente der Übertragungsmatrix zu ermitteln. Die Elemente der Übertragungsmatrix können verwendet werden, um den Übertragungsverlust der Probe sowie eine Reihe weiterer akustischer Eigenschaften zu berechnen. Die Vorgehensweise wird anhand der Ermittlung der akustischen Eigenschaften eines Fasermaterials demonstriert.

List of Symbols

c	ambient speed of sound
c_p	complex sound speed of the material under test
c_{ph}	phase speed of the material under test
G_{rr}	auto-spectrum of reference signal, r
H_{ir}	frequency response function between the complex sound pressure at the i-th microphone position and the complex reference signal, r
k	complex wave number in the ambient fluid
k_p	complex wave number of the material under test
P	complex sound pressure
$P\|_{x\,=\,0}$	sound pressure on the upstream face of the sample
$P\|_{x\,=\,d}$	sound pressure on the downstream face of the sample
R_a	normal incidence pressure reflection coefficient for the case of an anechoic termination
R_h	normal incidence pressure reflection coefficient for the hard backing case
t	time
T_a	normal incidence pressure transmission coefficient for the case of an anechoic termination
T_{ij}	transfer matrix element
TL_n	normal incidence transmission loss
V	complex normal acoustic particle velocity
$V\|_{x\,=\,0}$	acoustic particle velocity on the upstream face of the sample
$V\|_{x\,=\,d}$	acoustic particle velocity on the downstream face of the sample
Z_a	surface normal incidence impedance for the case of an anechoic termination
Z_p	complex characteristic impedance of the material under test

Greek

α_{na}	normal incidence absorption coefficient for the case of an anechoic termination
α_{nd}	normal incidence dissipation coefficient for the case of an anechoic termination
λ_p	wavelength within the material under test
ρ_0	ambient fluid density
ρ_p	complex density of the material under test
ω	angular frequency

Subscripts

a	case of an anechoic termination
h	hard backing case
n	normal incidence
p	material under test

Introduction

Many types of sound absorbing materials are used in noise control applications. These materials include, for example: glass fiber, polymeric fibrous materials, and various types of foams, along with barrier materials used either alone or in combination with absorbing layers to form composite treatments. It is of interest to be able to assess quickly the noise control impact of these materials, whether in sound absorption or barrier applications, as an aid either to material development or treatment selection. A procedure addressing that need is presented here. Although a primary result of the measurement procedure is the normal incidence transmission loss of the sample, a variety of other properties such as the ratio of the sound energy that is dissipated within the sample to the incident sound energy may also be determined.

The procedure described here represents an extension of work reported earlier by Bolton et al.[1] In that work, a four-microphone, standing wave tube measurement of the normal incidence reflection and transmission coefficients of automotive sealant materials was described. The success of that procedure depended on the provision of

a perfectly anechoic termination for the standing wave tube, which, in practice, is difficult if not impossible to assure. Even relatively small amounts of reflection from the termination could result in a noticeable distortion of the transmission loss. Here, it is shown that the same type of measured data may be used instead to determine the transfer matrix of the material under test if tests are conducted using two different tube termination (or loading) conditions. The procedure is thus referred to as a "two-load" method. The transfer matrix elements may then be related in closed form to the sample's normal incidence, anechoic transmission loss and other acoustical properties, all of which are independent of the tube termination conditions. Further, if the sample is a porous material that may be modeled as an effective fluid[2,13,23], that is, if its solid phase is perfectly rigid or perfectly limp, the sample's characteristic impedance and the complex wave number within it may also be determined. Note that the latter property in particular, yields both the phase speed and the spatial rate of energy dissipation within the material. Note also that when the transfer matrix of a sample is known, whether it be a homogeneous layer or a multi-layer composite, the transfer matrix may be combined with experimentally-derived or theoretically-predicted transfer matrices of other acoustical elements (for example, barrier or resistive layers) to form the transfer matrix of a complete, multi-layer noise control treatment.[3] The latter matrix may then be used to predict and optimise the absorption and barrier properties of the complete treatment.

Transfer matrix approaches have many applications in acoustics, and have also been used in hydraulics applications where this particular method is sometimes known as the two-port or four-pole method.[4] As a result, there is a large body of literature related to the measurement of the properties of acoustical elements based on transfer matrix, or two-port, representations.[5–11] The transfer matrix method adapted here for the measurement of material properties, has been widely used in the past both to analyze and to measure the acoustical properties of flow system elements (for example, automotive mufflers). In a measurement context, the transfer matrix estimation has most often been implemented in a two-load form. Also note, that the material property estimation procedure described here is of the same family as those described in references [5], and [12] to [18] in the sense that measurements are made on both sides of a cylindrical plug of material placed in a standing wave tube. However, this procedure differs from those referenced approaches in that knowledge of the tube termination condition is not required and because it is based more closely on techniques previously used to measure the acoustical performance of flow system components.

A measurement procedure that makes it possible to determine the transfer matrix of a sample that is symmetric front-to-back on the basis of a single measurement with a single, arbitrary-impedance tube termination (that is, a "one-load" method) has been described previously.[19] The one-load procedure is made possible by taking advantage of the reciprocal nature of sound transmission through symmetrical, homogeneous acoustical materials. That reciprocity imposes constraints on the structure of the transfer matrices of these materials. Those conditions have been noted previously by Pierce[20] and have been used earlier, without comment, by Bordone-Sacerdote and Sacerdote.[5] The mathematical constraints resulting from sample symmetry reduce the number of unknown transfer matrix elements from four to two, and thus make it possible to determine the acoustical properties of homogeneous and isotropic porous materials based on a single-load measurement, thus making it more convenient than the two-load approach when applied to appropriate materials. A summary of the one-load procedure is included here for the sake of completeness.

In this article, the theory underlying the transfer matrix approach is described first, then followed by a description of the experimental implementation of the procedure. Various measured results, including the normal incidence transmission loss along with corresponding reflection and absorption coefficients and surface normal impedances, are then presented for a nearly-homogeneous fibrous thermal insulation material. Based on the latter results, some further comments are offered on the frequency range over which useful experimental results may be obtained, in particular, over which frequency range the tube results may be taken to represent the properties of a laterally-infinite sample of the same material. It is noted that a low frequency limit is established by a sample resonance resulting from the constraint of the sample around its edges.

Theory of the Transfer Matrix Method

A. Sound Field Representation

In the approach considered here, it is assumed that the sound field in the up- and downstream segments of the standing wave tube can be well approximated by superpositions of positive- and negative-directed plane waves. In the frequency domain, the sound field can be written as:

$$P_{up} = Ae^{-jkx} + Be^{jkx} \tag{1a}$$

for the upstream segment, and:

$$P_{down} = Ce^{-jkx} + De^{jkx} \tag{1b}$$

for the downstream segment. Here k represents the wave number in the ambient fluid; P_{up} and P_{down} are complex sound pressures; and the coefficients A to D represent the complex amplitudes (Fig. 1). Note that an $e^{+j\omega t}$ sign convention has been adopted and is suppressed throughout the development.

Fig. 1. *Schematic of the standing wave tube*

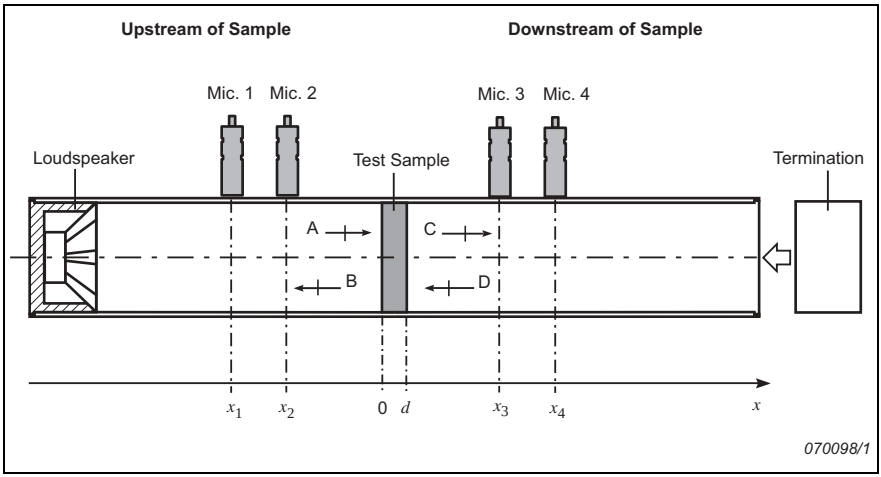

The complex sound pressures at the four measurement locations x_1 to x_4 can be written as:

$$P_1 = Ae^{-jkx_1} + Be^{jkx_1} \tag{2a}$$

$$P_2 = Ae^{-jkx_2} + Be^{jkx_2} \tag{2b}$$

$$P_3 = Ce^{-jkx_3} + De^{jkx_3} \tag{2c}$$

$$P_4 = Ce^{-jkx_4} + De^{jkx_4} \tag{2d}$$

Equations (2a) to (2d) yield four equations for the coefficients A to D in terms of the four measured sound pressures:

$$A = \frac{j\left(P_1 e^{jkx_2} - P_2 e^{jkx_1}\right)}{2\sin k(x_1 - x_2)} \tag{3a}$$

$$B = \frac{j\left(P_2 e^{-jkx_1} - P_1 e^{-jkx_2}\right)}{2\sin k(x_1 - x_2)} \tag{3b}$$

$$C = \frac{j\left(P_3 e^{jkx_4} - P_4 e^{jkx_3}\right)}{2\sin k(x_3 - x_4)} \tag{3c}$$

$$D = \frac{j\left(P_4 e^{-jkx_3} - P_3 e^{-jkx_4}\right)}{2\sin k(x_3 - x_4)} \tag{3d}$$

The latter coefficients provide the input data for subsequent transfer matrix calculations. Note that the wave number, k, should be made complex to account for the effects of viscous and thermal dissipation in the oscillatory, thermoviscous boundary layer that forms on the inner surface of the duct. In the present work, a semi-empirical formula given by Temkin was used to calculate the real and imaginary parts of the wave number.[22]

B. Transfer Matrix Formulation

The complex coefficients A to D can be used to calculate the sound pressures and particle velocities at the two surfaces of the sample. The latter quantities can then be related to each other by a two-by-two transfer matrix, and it is shown in this subsection that the elements of that transfer matrix can be determined based on the sound

pressure measurements at the four microphones. The latter is important, since the acoustical properties of the sample are completely defined once the transfer matrix elements are known. That is, based on a knowledge of the transfer matrix, the transmission loss of the sample may be determined for arbitrary tube termination conditions.

Thus, a transfer matrix is used to relate the sound pressures and normal acoustic particle velocities on the two faces of a sample extending from $x = 0$ to $x = d$, as in Fig. 1:

$$\begin{bmatrix} P \\ V \end{bmatrix}_{x=0} = \begin{bmatrix} T_{11} & T_{12} \\ T_{21} & T_{22} \end{bmatrix} \begin{bmatrix} P \\ V \end{bmatrix}_{x=d} \tag{4}$$

In Eq. (4), P is the exterior sound pressure and V is exterior, normal acoustic particle velocity. The pressures and particle velocities at the two surfaces of the porous layer may easily be expressed in terms of the positive- and negative-going plane wave component amplitudes: that is,

$$P\big|_{x=0} = A + B \tag{5a}$$

$$V\big|_{x=0} = \frac{A - B}{\rho_0 c} \tag{5b}$$

$$P\big|_{x=d} = Ce^{-jkd} + De^{jkd} \tag{5c}$$

$$V\big|_{x=d} = \frac{Ce^{-jkd} - De^{jkd}}{\rho_0 c} \tag{5d}$$

where ρ_0 is the ambient fluid density and c is the ambient sound speed. Thus when the plane wave components are known, based on measurements of the complex pressures at four locations, the pressures and the normal particle velocities at the two surfaces of the porous layer can be determined.

It is then of interest to determine the elements of the transfer matrix since, as will be shown below, the elements of that matrix may be directly related to the properties of the sample. However, first note that Eq. (4) represents two equations in four unknowns: T_{11}, T_{12}, T_{21} and T_{22}. Thus, two additional equations are required in order to be able to solve for the transfer matrix elements. Those equations may be generated by making a second, independent measurement at the four microphone positions after changing the impedance terminating the downstream section of the standing wave tube. That approach is the basis of the so-called two-load method.[8] In matrix form, the result of the two independent measurements may be expressed as:

$$\begin{bmatrix} P_1 & P_2 \\ V_1 & V_2 \end{bmatrix}_{x=0} = \begin{bmatrix} T_{11} & T_{12} \\ T_{21} & T_{22} \end{bmatrix} \begin{bmatrix} P_1 & P_2 \\ V_1 & V_2 \end{bmatrix}_{x=d} \tag{6}$$

where the subscripts 1 and 2 on the pressures and particle velocities, denote the two different termination conditions. The transfer matrix elements may then be determined by inverting the latter expression to obtain

$$\begin{bmatrix} T_{11} & T_{12} \\ T_{21} & T_{22} \end{bmatrix} = \frac{1}{P_1\big|_{x=d} V_2\big|_{x=d} - P_2\big|_{x=d} V_1\big|_{x=d}} \times \tag{7}$$

$$\times \begin{bmatrix} P_1\big|_{x=0} V_2\big|_{x=d} - P_2\big|_{x=0} V_1\big|_{x=d} - P_1\big|_{x=0} P_2\big|_{x=d} + P_2\big|_{x=0} P_1\big|_{x=d} \\ V_1\big|_{x=0} V_2\big|_{x=d} - V_2\big|_{x=0} V_1\big|_{x=d} - P_2\big|_{x=d} V_1\big|_{x=0} + P_1\big|_{x=d} V_2\big|_{x=0} \end{bmatrix}$$

Under certain circumstances, it is possible to take advantage of the reciprocal nature of a sample to generate two additional equations instead of making a second set of measurements. Pierce noted that reciprocity requires that the determinant of the transfer matrix be unity.[20] Ingard has noted that the latter constraint is a general property of passive, linear four-pole networks.[13] Allard has also shown that this condition follows directly from the requirement that the transmission coefficient of a planar, arbitrarily-layered acoustical system be the same in both directions.[23] Further, Pierce notes that for symmetrical systems, $T_{11} = T_{22}$. It may easily be shown that the latter condition follows when the plane wave reflection coefficients from the two surfaces of a planar, layered system are the same.[19] Thus, given reciprocity and symmetry, it follows that:

$$T_{11} = T_{22} \tag{8a}$$

$$T_{11}T_{22} - T_{12}T_{21} = 1 \tag{8b}$$

The latter two constraint conditions along with a single measurement for one tube termination condition complete the set of four equations necessary to solve for the transfer matrix elements. Specifically, by combining Eqs. (4), (8a) and (8b), the transfer matrix elements for a sample satisfying the above conditions can be expressed directly in terms of the pressures and velocities on the two surfaces of the porous layer for one termination condition: that is,

$$\begin{bmatrix} T_{11} & T_{12} \\ T_{21} & T_{22} \end{bmatrix} = \frac{1}{P|_{x=0}V|_{x=d} + P|_{x=d}V|_{x=0}} \times \tag{9}$$

$$\times \begin{bmatrix} P|_{x=d}V|_{x=d} + P|_{x=0}V|_{x=0} & P|_{x=0}^2 - P|_{x=d}^2 \\ V|_{x=0}^2 - V|_{x=d}^2 & P|_{x=d}V|_{x=d} + P|_{x=0}V|_{x=0} \end{bmatrix}$$

The latter procedure will be referred to here as the one-load method.

Once the transfer matrix elements are obtained by using either the one- or two-load methods, all of the other acoustical properties of a sample, for example, its reflection and transmission coefficients, can be calculated, as will be demonstrated next.

C. Calculation of Reflection and Transmission Coefficients

For example, consider a sample of depth d backed by a perfectly anechoic termination, so that it can be assumed that D is identically zero in the downstream tube section. When the incident plane wave is assumed to have unit amplitude, the sound pressures and particle velocities on the two surfaces of the porous layer become:

$$P|_{x=0} = 1 + R_a \tag{10a}$$

$$V|_{x=0} = \frac{1 - R_a}{\rho_0 c} \tag{10b}$$

$$P\big|_{x=d} = T_a e^{-jkd} \tag{10c}$$

$$V\big|_{x=d} = \frac{T_a e^{-jkd}}{\rho_0 c} \tag{10d}$$

where $R_a = B/A$ and $T_a = C/A$ are the normal incidence, plane wave reflection and transmission coefficients, respectively, for an anechoically-terminated sample. When Eqs. (10a), (10b), (10c) and (10d) are substituted into Eq. (4), the normal incidence pressure transmission and reflection coefficients for the case of an anechoic termination, T_a and R_a, respectively, are found to be:

$$T_a = \frac{2e^{jkd}}{T_{11} + \frac{T_{12}}{\rho_0 c} + \rho_0 c T_{21} + T_{22}} \tag{11}$$

$$R_a = \frac{T_{11} + \frac{T_{12}}{\rho_0 c} - \rho_0 c T_{21} - T_{22}}{T_{11} + \frac{T_{12}}{\rho_0 c} + \rho_0 c T_{21} + T_{22}} \tag{12}$$

In addition, the surface normal impedance of the anechoically terminated sample may be calculated as:

$$Z_a = \frac{T_{11} + T_{12}/\rho_0 c}{T_{21} + T_{22}/\rho_0 c} \tag{13}$$

In contrast, when the sample of depth d is positioned against a rigid backing, then $V\big|_{x=d} = 0$. When the latter condition and Eqs. (10a) and (10b) are substituted into Eq. (4), the normal incidence reflection coefficient for the hard backing case, R_h, is obtained as:

$$R_h = \frac{T_{11} - \rho_0 c T_{21}}{T_{11} + \rho_0 c T_{21}} \tag{14}$$

Similar expressions may easily be derived for the case of a porous layer backed by an arbitrary impedance.

The normal incidence transmission loss of a sample can be calculated as:

$$TL = 10 \log \frac{1}{|T_a|^2} \tag{15}$$

Note that when the same fluid is on both sides of the sample, $|T_a|^2$ is the normal incidence, power transmission coefficient for an anechoically-terminated sample. That is, the ratio of the sound power transmitted by the sample to the sound power incident on the sample. In the case of a perfectly anechoic termination, $D = 0$, and $T_a = C/A$. Note, however, that the sound power transmitted by a sample depends in general both on the properties of the sample and on the tube termination conditions. For example, in the extreme case of a perfectly rigid termination, the plane wave coefficients C and D are equal in magnitude and the sound power transmitted by the sample is, in principle, zero, thus causing the transmission loss to be apparently infinite. Even when a tube termination is "nearly-anechoic", small reflections from the termination may have a noticeable impact on the transmission coefficient if it is calculated simply as C/A.[1] A major advantage of the transfer matrix approach presented here is that the transfer matrix elements are properties only of the sample and not of the measurement environment. Further, when those elements are known, the sound power transmitted by the sample can be calculated for any tube termination condition. When the latter calculation is based on a perfectly anechoic termination, as in Eq. (11), the corresponding transmission loss gives a true indication of the sample's barrier performance.

D. Calculation of Wave Number and Characteristic Impedance

Next, note that the normal incidence transfer matrix for a finite-depth layer of a homogeneous, isotropic porous material that it can be considered to be either limp or rigid so that it can be modeled as an equivalent fluid is:[13, 23]

$$\begin{bmatrix} T_{11} & T_{12} \\ T_{21} & T_{22} \end{bmatrix} = \begin{bmatrix} \cos k_p d & j\rho_p c_p \sin k_p d \\ j \sin k_p d / \rho_p c_p & \cos k_p d \end{bmatrix} \tag{16}$$

In Eq. (16), k_p is the complex wave number in the acoustical material; d is the layer thickness; and $\rho_p c_p$ is the complex characteristic impedance of the material. Thus, the four transfer matrix elements may be directly associated with the acoustical properties of the porous material. In particular, the wave number can be evaluated either as:

$$k_p = \frac{1}{d} \cos^{-1} T_{11} \tag{17a}$$

or

$$k_p = \frac{1}{d} \sin^{-1} \sqrt{-T_{12} T_{21}} \tag{17b}$$

and the characteristic impedance of the acoustical material can be calculated most directly as:

$$\rho_p c_p = \sqrt{\frac{T_{12}}{T_{21}}} \tag{18}$$

Quantities such as the complex sound speed, $c_p = \omega / k_p$, and complex density, $\rho_p = \rho_p c_p / c_p$, can easily be determined when k_p and $\rho_p c_p$ are known.

Experimental Procedure

The experimental procedure described here is based very closely on the earlier work by Song and Bolton.[19] The measurements were made using Brüel & Kjær's Transmission Loss Tube Kit Type 4206-T. A loudspeaker at one end of the tube was used to generate a broadband random signal over the frequency range 0 to 6400 Hz, and the frequency response functions between the input signal to the loudspeaker and the complex sound pressures at each of the four measurement positions were measured simultaneously by using Brüel & Kjær's Pulse FFT & CPB Analysis Type 7700 software running on a personal computer. Coefficients A to D can then be estimated by using the following formulae:

$$A = \sqrt{G_{rr}}\,\frac{j\left(H_{1r}e^{jkx_2} - H_{2r}e^{jkx_1}\right)}{2\sin k(x_1 - x_2)} \tag{19a}$$

$$B = \sqrt{G_{rr}}\,\frac{j\left(H_{2r}e^{-jkx_1} - H_{1r}e^{-jkx_2}\right)}{2\sin k(x_1 - x_2)} \tag{19b}$$

$$C = \sqrt{G_{rr}}\,\frac{j\left(H_{3r}e^{jkx_4} - H_{4r}e^{jkx_3}\right)}{2\sin k(x_3 - x_4)} \tag{19c}$$

$$D = \sqrt{G_{rr}}\,\frac{j\left(H_{4r}e^{-jkx_3} - H_{3r}e^{-jkx_4}\right)}{2\sin k(x_3 - x_4)} \tag{19d}$$

where H_{ir} is the frequency response function between the complex sound pressures, P_i, and the complex reference signal, r, provided for the loudspeaker; and G_{rr} is the autospectrum of reference signal, r.

In this approach, it is assumed that the loudspeaker is perfectly linear, which may be confirmed by an inspection of the coherence of the frequency response functions as a function of source level. If only four data acquisition channels are available, the signal from microphone 1 may be used as the reference.[27]

Brüel & Kjær Transmission Loss Kit Type 4206-T (Fig. 2) is suitable for both low frequency (50 to 1600 Hz) and high frequency (500 to 6400 Hz) measurements since it includes both 2.9 cm and 10.0 cm inner diameter tube sections. In principle, it is necessary to compensate for the propagation delay between the loudspeaker and the various microphones to avoid the introduction of a time delay bias error which can result in a uniform reduction of the coherence.[27,26] In practice, compensation is not necessary when the propagation delays are very small compared to the time record lengths used to compute the cross-spectral and transfer function estimates.

The transmission loss tubes feature microphone holders positioned both up- and downstream of a sample holder having the same inner diameter as the up- and downstream sections, see Fig. 2.

Fig. 2. *Schematic of Type 4206-T*

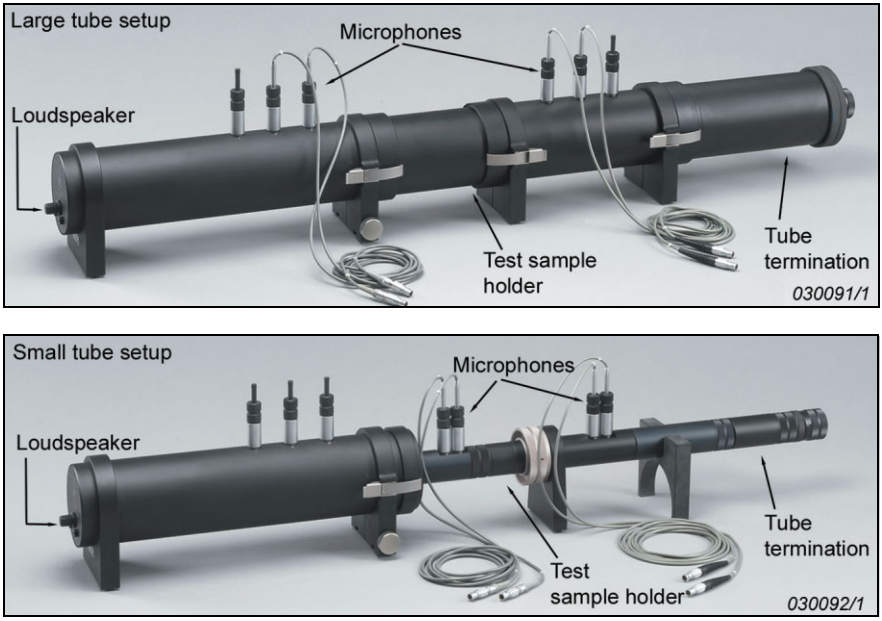

The two measurement positions in the up- and downstream tube sections were separated by a distance of 5 cm for the large tube and 2 cm for the small tube. Note that it has been reported that there is a frequency-dependent, optimum microphone

separation for multi-microphone measurements of the type reported here.[28] The latter effect could be important under poor signal-to-noise conditions.

For the two-load measurement cases, measurements were made first with the tube termination open, and then when the downstream tube sections were terminated by approximately anechoic terminations. The latter were created by loosely packing the standard sample holders with an approximately 70 cm depth of 3 M Thinsulate™ sound absorbing material. The absorption coefficients of the large and small tube terminations are plotted in Fig. 3.

Fig. 3. *Absorption coefficients of nearly anechoic terminations.* ***(a):*** *Large tube. Frequency range: 20 Hz – 1.6 kHz,* ***(b):*** *Small tube. Frequency range: 20 Hz – 6.4 kHz*

3a.

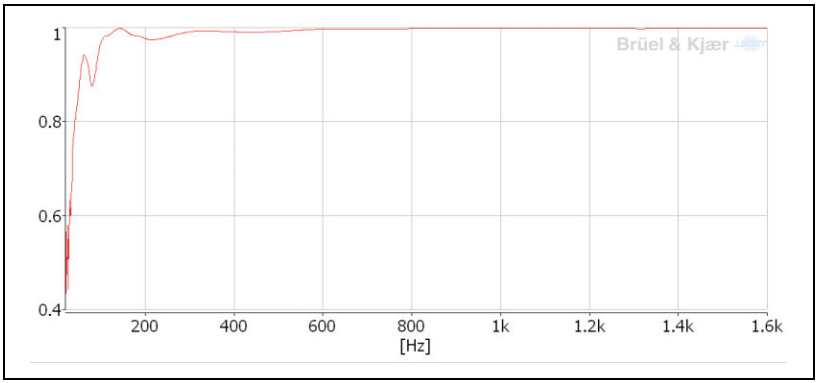

3b.

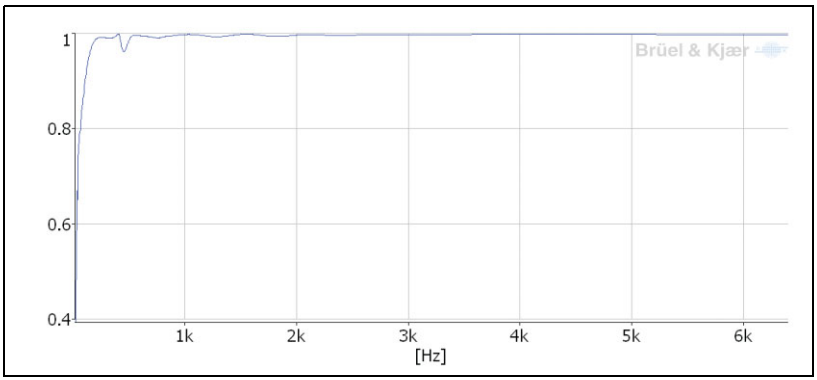

In the one-load measurement case, the measurements were performed with the anechoic terminations in place. Note that an anechoic termination is not required by either of the two- or one-load measurement procedures discussed in the last section.

In principle, the termination impedance can be arbitrary, and its value need not be known. However, the presence of the anechoic termination in at least one measurement condition causes the sound field in the downstream section to be almost purely propagational in that case, thus maximising the phase difference between the sound pressures at the two downstream microphone locations and minimising the effect of microphone phase-mismatch on the downstream transfer function estimates. Note that a microphone switching procedure may be performed at a calibration stage to reduce the effects of microphone and measurement channel mismatch, as recommended in ASTM standard E 1050, for example.[29] Owing to the type of test material considered here (that is, highly absorptive), the measurement environment in the tube was not difficult and the microphone switching procedure had a negligible impact on the results. Thus, all the results shown in the next section were calculated without using a microphone switching procedure. Note also that when the downstream termination impedance is known either a priori (for example, if there is a rigid termination) or by independent measurement, the relation between the coefficients C and D in Eqs. (2a) to (2d) can be determined. In that case only a single downstream sound pressure measurement would be required, and the one-load procedure described above would become, in effect, a broadband implementation of the Champoux and Stinson technique described in reference [15].

The material used in the present tests was a fibrous, thermal insulation material provided by 3 M Corporation and is denoted THL. The properties of THL are listed in Table 1. Cylindrical samples of the material were carefully cut to fit snugly inside the sample holder. Care was taken to ensure that there were no leaks around the circumference of the samples and that the samples were not deformed when placed in the tube. The measurements were made using either three or six layers of material to give total sample thicknesses of 11.1 cm and 22.2 cm. Lining materials were carefully inserted into the sample holder so that the depth of the individual layers comprising the complete sample was preserved. To reduce the effect of sample mounting variability and material inhomogeneity, multiple transmission measurements were performed using a total of thirty individual samples. For the three layer measurements, ten sets of three samples were measured; for the six layer measurements, five groups of six samples were used. In the small tube measurements, the samples were positioned so that their front surface was 3.5 cm downstream of microphone 2, and so that there was a 16.5 cm distance from the front of the sample to microphone 3. In the large tube case, the front surface of the sample was positioned 15 cm downstream of microphone 2, and 30 cm upstream of microphone 3. It is generally recommended that the sample surfaces be no closer than

one tube diameter from the closest microphone position to ensure that non-propagating modes induced by sample inhomogeneity and edge constraints do not contribute to the measured sound pressures.

Table 1. The physical properties of THL

Thickness	Mass Per Unit Area
3.7 cm (single layer of THL)	0.156 Kg/m^2

Results and Discussion

A. Transfer Matrix

The magnitudes and phases of the averaged transfer matrix elements for the THL materials, calculated using Eq. (7), are plotted in Fig. 4. These results are based on a two-load measurement using three layers of material. Each of the elements is significant in this case, and each has a particular physical meaning. Note first that the elements T_{11} and T_{22} are identical for practical purposes, owing to the fact that the sample was essentially homogeneous and symmetric, back-to-front. As a consequence, the one-load and two-load estimates of the transmission loss of this sample are almost identical, as will be discussed in the next sub-section. Further, the element T_{11} is the ratio of the upstream and downstream pressures in the case of a zero velocity state at the downstream layer surface, and it is thus dimensionless. The element T_{12} is the ratio of the upstream pressure and downstream velocity when a zero pressure state exists at the downstream surface of the sample, and thus it has the units of impedance. Conversely, T_{21} represents the ratio of the upstream velocity and the downstream pressure when the downstream surface velocity state is zero, that is, for the case of a hard-backing boundary condition at the downstream surface of the sample. The element T_{21} thus has the units of admittance.

Fig. 4. *Averaged transfer matrix elements, T_{ij}, for three layers of THL material based on a two-load measurement in the small tube for both magnitude and phase. Frequency range: 50 Hz – 6.4 kHz. Dotted curves: Standard deviation (±1).* ***(a):*** T_{11}, ***(b):*** T_{12}, ***(c):*** T_{21}, ***(d):*** T_{22}

4a.

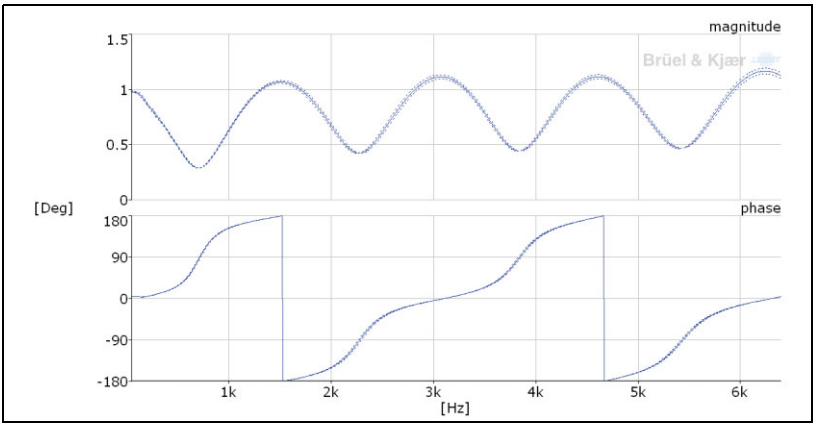

4b.

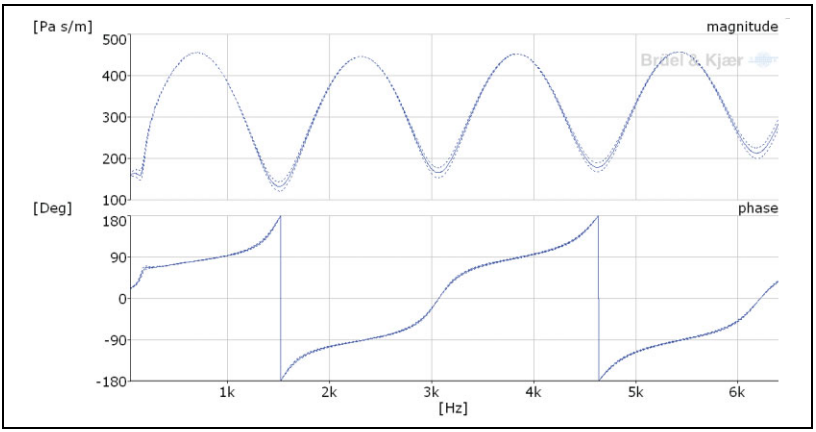

4c.

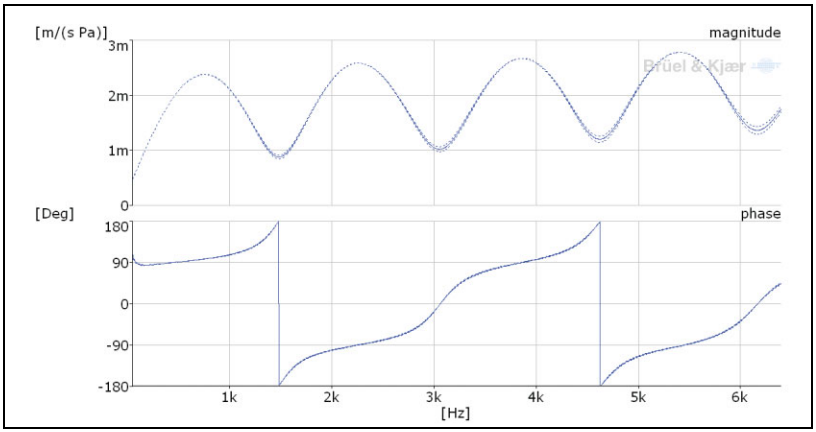
[m/(s Pa)]
magnitude
3m
2m
1m
0
Brüel & Kjær
[Deg]
phase
180
90
0
-90
-180
1k
2k
3k
4k
5k
6k
[Hz]

4d.

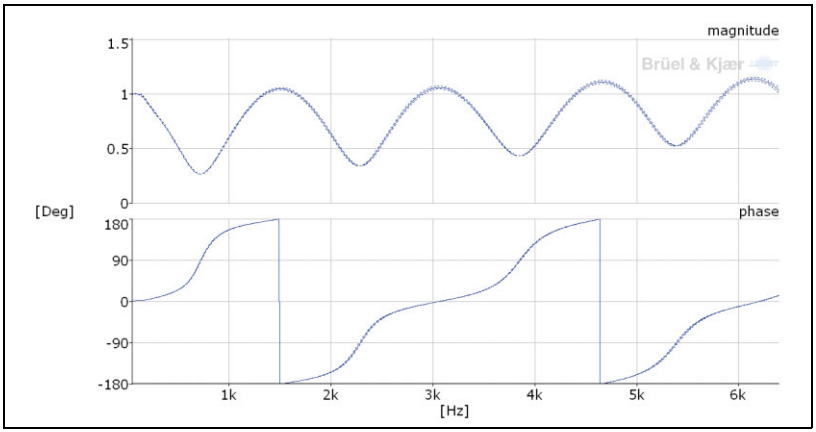
magnitude
1.5
1
0.5
0
Brüel & Kjær
[Deg]
phase
180
90
0
-90
-180
1k
2k
3k
4k
5k
6k
[Hz]

B. *Transmission Loss*

Consider next the normal incidence transmission loss of both three and six layer samples calculated using Eqs. (11) and (15): see Fig. 5 to Fig. 9. The results of both one- and two-load measurements for 3 layers of material are shown in Fig. 5 for both the large tube and small tubes. It can be seen that the transmission loss increases monotonically with increasing frequency above 200 Hz as would be expected for a porous layer.Note also that there are resonance features at approximately 40 and 120 Hz in the large tube results, and at approximately 150 and 450 Hz in the small tube results. This behaviour is typical of the effect of sample edge constraint on the normal incidence transmission loss of an elastic porous material,[1,31,32,33,34] an effect first noted by Beranek in the context of normal incidence absorption measurements.[30] The two features represent the effects of the first two diaphragm-like modes of the samples in which the sample experiences a pure shearing motion.[31,32] The frequencies at which these features occur are inversely proportional to the sample diameter and are directly proportional to the square root of the ratio of the shear modulus and density of the sample. Thus, the first resonance in the large tube case occurs at approximately one-quarter of the resonance frequency observed in the small tube. Further, this effect is primarily significant at low frequencies owing to the relatively strong viscous coupling between the solid and fluid phases of the porous material in that region. At frequencies below the first resonance, the transmission loss, in principle, rises to a low-frequency limit proportional to the flow resistance of the sample.[31,32] The latter behaviour is not clearly evident for the present material since its shear modulus is relatively low, with the result that the first diaphragm-like mode occurs at very low frequencies. In this region the microphone separations in the upstream and downstream pairs are very small compared to a wavelength, so that the measurements may not be particularly accurate owing to the effect of residual phase mismatch between the microphones. Nonetheless, a close examination of the data shows that the transmission loss does indeed increase with decreasing frequency below the first resonance in both the large and small tube results. Thus, at low frequencies the sample edge constraint causes the normal incidence transmission loss of a porous sample measured in a tube to differ from that of a laterally infinite plane sheet of the same material. This effect becomes more significant as the flow resistivity of the samples increases (therein increasing the strength of the coupling between the solid and fluid phases of the material) and the shear stiffness of the sample increases in proportion to its bulk density (increasing the frequency of the diaphragm-like resonances). This effect is particularly noticeable in measurements of

essentially impermeable barrier materials, which may also be tensioned when they are held in the sample holder.

Fig. 5. *Averaged normal incidence transmission loss, TL_n, for three layers of THL material with standard deviations (dotted curves) measured using one- and two-load methods. Red curves: One-load method. Blue curves: Two-load method.* ***(a):*** *Results from large tube. Frequency range: 20 Hz – 1.6 kHz,* ***(b):*** *Results from small tube. Frequency range: 20 Hz – 6.4 kHz*

5a.

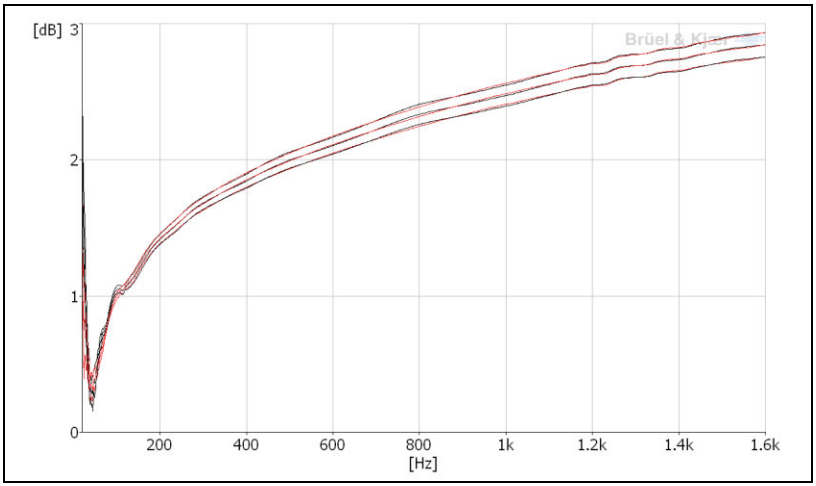

5b.

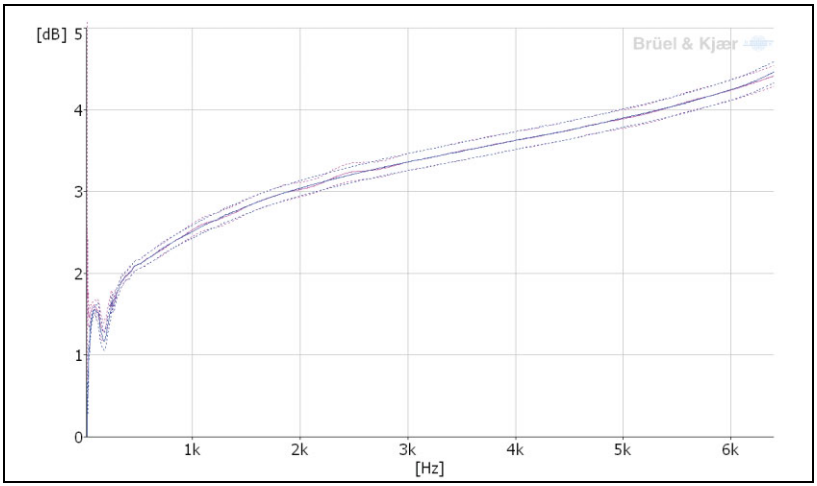

The data shown in Fig. 5 also indicate that the one- and two-load methods give essentially the same results in this case, as would be expected owing to the symmetry of the sample. At low frequencies, the effects of noise are more clearly evident in the one-load method results and at higher frequencies the variation of the transmission loss with frequency is not as smooth in the one-load case as for the two-load case.

In Fig. 6, the transmission losses measured for three-layer samples in both the large and small tubes are superimposed.

Fig. 6. *Averaged normal incidence transmission loss, TL_n, for three layers of THL material with standard deviations (dotted curves). Red curves: Large tube. Blue curves: Small tube.* ***(a):*** *Frequency range: 20 Hz – 1.6 kHz,* ***(b):*** *Frequency range: 20 Hz – 6.4 kHz*

6a.

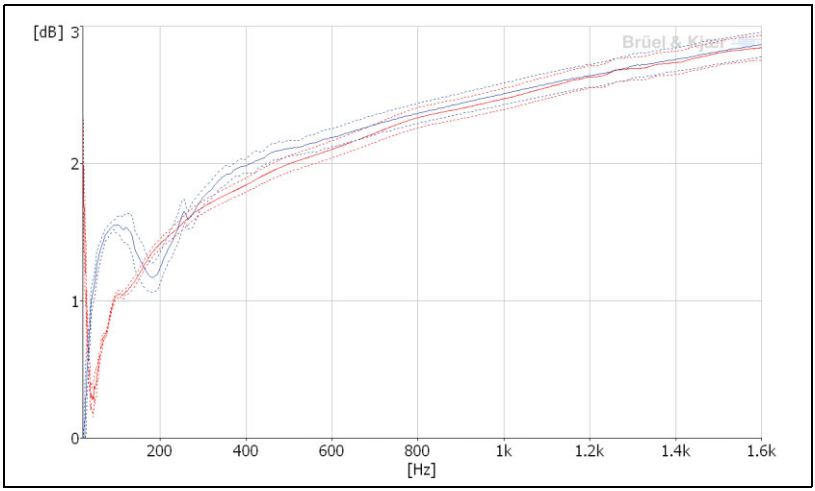

6b.

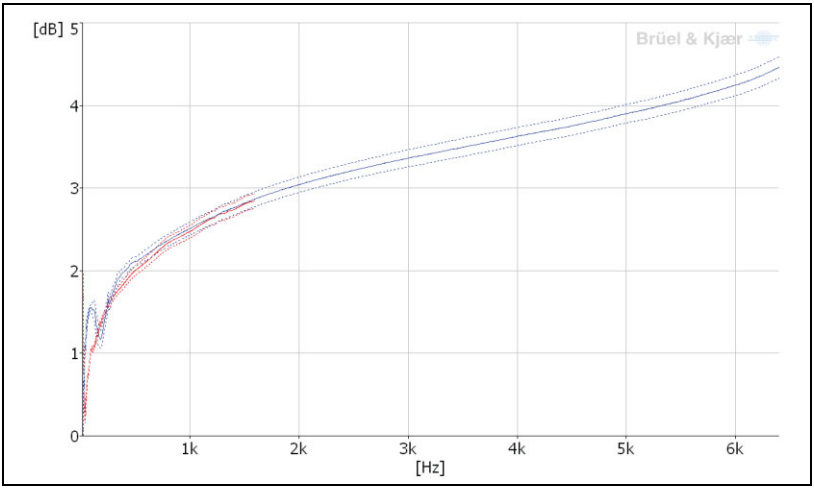

Nonetheless, the results of the two methods are, for practical purposes, the same for this material. The differences between the two results are generally much less than the standard deviation of the measurement (resulting from sample and sample mounting variability). Thus, for samples that are, practically-speaking, symmetric, the one-load method may be used as a matter of convenience, if desired.

In the two-load results for the large and small tubes shown in Fig. 6, it may be seen there that there is excellent agreement between the two sets of results in the frequency range in which they overlap – except at the lowest frequencies, in which region the edge-constraint effect discussed above causes the results to differ from one another. However, for this material, the difference between the two measurements in the frequency range from approximately 200 to 1600 Hz is generally less than the standard deviation of the results. Thus, if edge-constraint effects are not an issue either in the upper frequency range of the large tube results or the low frequency range of the small tube results, satisfactory overlap of the measurements may be expected.

Finally, in Fig. 7, the transmission loss results for three and six layers of material measured in the large tube are compared. There it may be seen that the transmission loss of the six layer samples is very nearly equal to twice the transmission loss of the three layer samples (also plotted) as would be expected for a uniform material. Again, the difference between the directly measured six-layer result and that estimated by simply doubling the transmission loss of the three-layer sample is smaller than the standard deviation of the results.

Fig. 7. *Averaged normal incidence transmission loss, TL_n, for three and six layers of THL material with standard deviations (dotted curves). Frequency range: 50 Hz – 1.6 kHz. Red curves: Three layers. Green curves: Six layers. Blue curves: 2 × three layers*

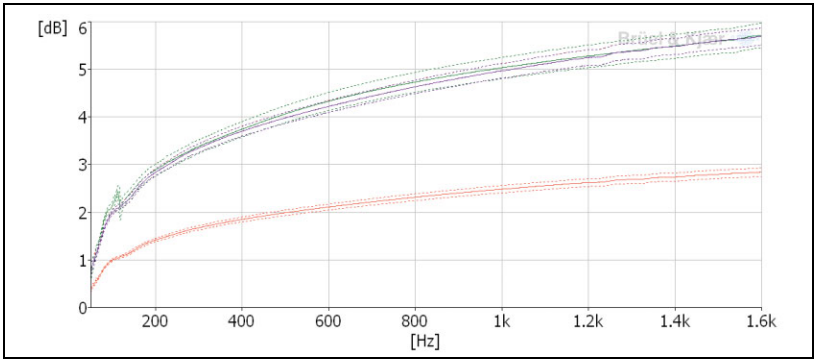

Note that the transmission loss discussed in this section is the normal incidence transmission loss, which generally differs from the random incidence transmission loss that is typically measured using a sample placed between two reverberation rooms.[35] There is no simple relationship between the random and normal incidence transmission except for particular types of materials. For example, if the sample is a homogeneous, isotropic porous material that is either perfectly limp or rigid, the random incidence transmission loss may be calculated from a knowledge of the sample's complex density and sound speed (see sub-section "Complex Density and Sound Speed" on page 37).[36]

C. Reflection and Absorption Coefficients and Surface Normal Impedance

The reflection and absorption coefficients along with the surface normal impedance of the three layer samples measured in both the small and large tubes are shown in Fig. 8 to Fig. 11, and will be discussed briefly here.

The plane wave, anechoic reflection coefficient, R_a, was calculated using Eq. (11), and is shown in Fig. 8. Since the flow resistance of the material under test was relatively low, and because the sample was effectively anechoically-terminated, most of the incident energy was either transmitted through the sample or was dissipated within it. As a result, the magnitude of the reflection coefficient is relatively low except at the lowest frequencies where the sample is stiffened by the effect of the edge constraint. Note that the feature in the small tube reflection

coefficient near 200 Hz is associated with edge-constraint resonance discussed in the last sub-section.

Fig. 8. *Averaged normal incidence anechoic reflection coefficient, R_{na}, for three layers of THL material with standard deviations (dotted curves). Red curves: Large tube. Blue curves: Small tube.* ***(a):*** *Frequency range: 20 Hz – 1.6 kHz,* ***(b):*** *Frequency range: 20 Hz – 6.4 kHz*

8a.

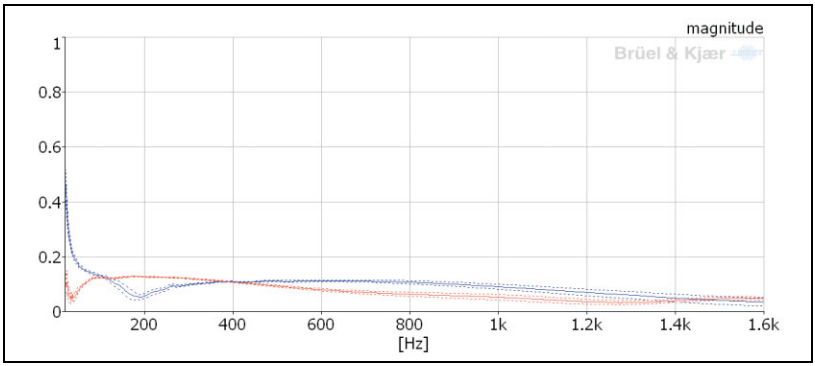

8b.

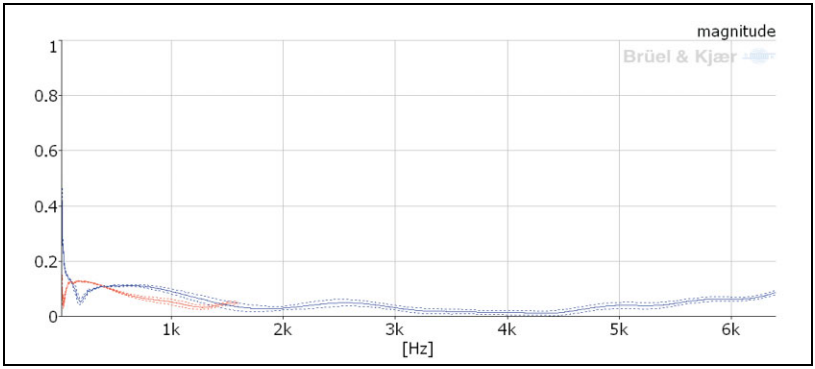

The normal incidence, anechoic absorption coefficients for the small and large tube cases were calculated as:

$$\alpha_{na} = 1 - \left|R_a\right|^2 \tag{20}$$

and are shown in Fig. 9.

Fig. 9. *Averaged normal incidence anechoic absorption coefficient, α_{na}, for three layers of THL material with standard deviations (dotted curves). Red curves: Large tube. Blue curves: Small tube.* ***(a):*** *Frequency range: 20 Hz – 1.6 kHz,* ***(b):*** *Frequency range: 20 Hz – 6.4 kHz*

9a.

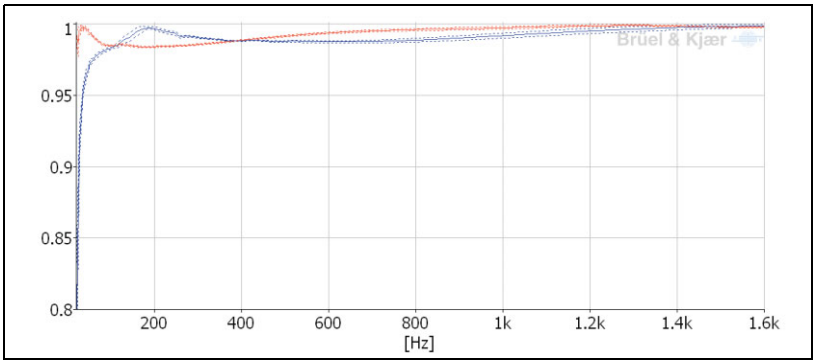

9b.

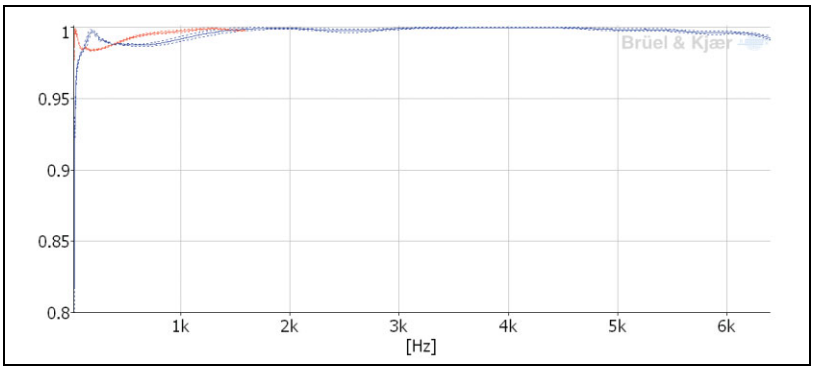

It may be seen, as expected, that the absorption coefficients are nearly unity, except at the lowest frequencies. An interesting feature of the method, is that it is possible to distinguish the fraction of the incident energy that is dissipated within the sample, from that that is simply transmitted through it. Here we define the normal incidence, anechoic dissipation coefficient as:

$$\alpha_{nd} = 1 - \left|R_a\right|^2 - \left|T_a\right|^2 = \alpha_{na} - \left|T_a\right|^2 \tag{21}$$

that is, as the difference between the fraction of the incident energy absorbed by the sample at its front surface and transmitted at its rear surface. The dissipation

coefficient is, therefore, a measure of the sample material's ability to dissipate energy. The dissipation coefficients for the three layer samples in the large and small tube are shown in Fig. 10, where it can be seen that the dissipation within the sample increases essentially monotonically with frequency, as is typical for a porous material.

Fig. 10. *Averaged dissipation coefficient, α_{nd}, for three layers of THL material with standard deviations (dotted curves). Red curves: Large tube. Blue curves: Small tube.*
(a): *Frequency range: 20 Hz – 1.6 kHz,* ***(b):*** *Frequency range: 20 Hz – 6.4 kHz*

10a.

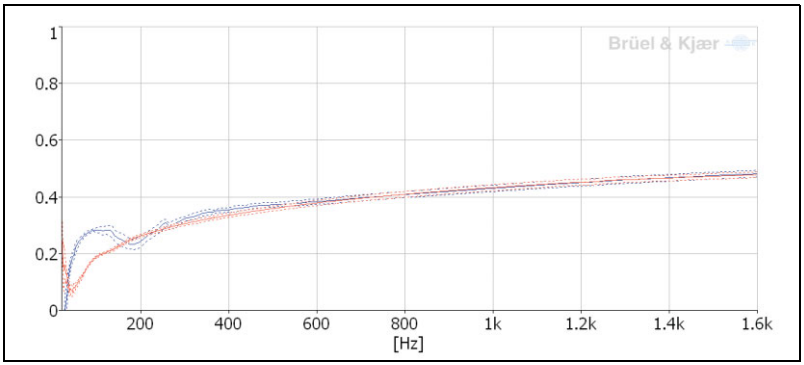

10b.

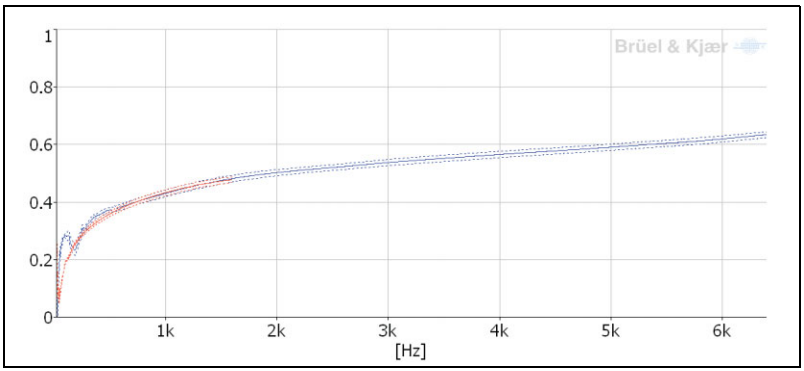

The surface normal impedance of the anechoically terminated sample was calculated using Eq. (13) and the large and small tube results are shown in Fig. 11.

Fig. 11. *Averaged surface normal impedance in the case of anechoic termination, Z_a, for three layers of THL material with standard deviations (dotted curves). Red curves: Large tube. Blue curves: Small tube.* ***(a):*** *Frequency range: 20 Hz – 1.6 kHz,* ***(b):*** *Frequency range: 20 Hz – 6.4 kHz*

11a.

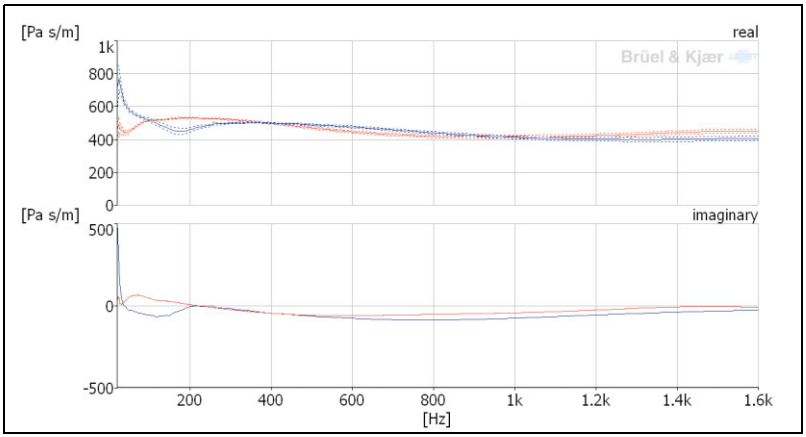

11b.

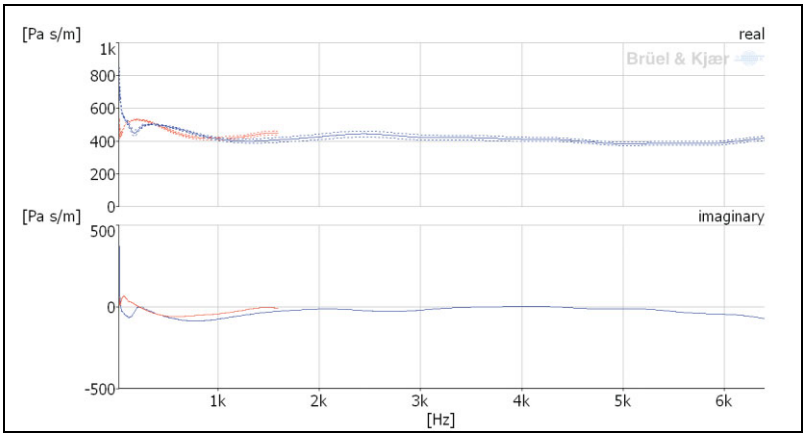

Note that over most of the frequency range, the real part of the normal impedance is only slightly greater than $\rho_0 c$, and the imaginary part is relatively small, which is consistent with the high levels of absorption noted previously. It should be emphasised that the absorption coefficient of an anechoically terminated sample is significantly different (and usually larger) than the absorption of the

same sample when rigidly-backed as would normally be measured in a two-microphone standing wave tube.

D. Wave Number and Characteristic Impedance

Many types of sound absorbing materials are used in noise control applications. It is of interest to be able to predict the noise control impact of these materials, whether in sound absorption or barrier applications. At the design stage, finite element, boundary element and statistical energy analysis programmes make that possible in principle. However, to take full advantage of these software capabilities, it is necessary to have detailed knowledge of the acoustical properties of the noise control materials. In particular, it is usually necessary to know their characteristic impedance and wave number.

In this sub-section we will imagine that the porous materials under test are homogeneous (that is, materials whose properties are spatially uniform) and isotropic (materials whose properties are independent of direction), and that their expanded solid phase may be assumed to be either perfectly rigid or perfectly limp. In general, most noise control materials are poroelastic: that is, they can support two compressional waves and a transverse wave.[37] However, in certain frequency or material property regimes, certain porous materials behave as though they were rigid, in that their solid phase motion is negligible compared to that of the fluid phase owing to weak coupling or the relatively high density or stiffness of the solid phase. In other regimes, certain materials such as low density, high flow resistivity, unreinforced glass fibers may be approximated as being limp, meaning that the in vacuo stiffness of their bulk solid phase is negligible compared to that of the saturating fluid.[3] For practical purposes, many fibrous materials and foams fall into these two categories in specific frequency ranges of interest. Air-saturated, homogeneous and isotropic porous materials that can be approximated as either rigid or limp may be considered to support only a single dilational wave type and may thus be modeled as dissipative fluids having complex physical properties, for example, characteristic impedance and wave number.[2] The acoustical properties of such a medium are completely specified when the latter two quantities, or two independent properties derived from them (such as complex density and complex sound speed) are known. Thus, it is of interest to be able to determine experimentally the wave number and the characteristic impedance of a homogeneous and isotropic porous material. Further, note that when the medium can be modeled as an effective fluid, the acoustical properties of a laterally infinite layer of that material are completely specified by a two-by-two transfer matrix.

The material considered here, THL, may be modeled as an effective fluid since the motion of its solid phase is essentially negligible owing to the material's relatively low flow resistivity. The wave numbers and normalised characteristic impedances for the THL material are plotted in Fig. 12 and Fig. 13, respectively. Those results are based on three-layer, two-load measurements. The real part of the wave number is a measure of the rate of change of phase with position within the porous material, and increases with frequency approximately, but not quite linearly (owing to the variation of wave speed with frequency within the material). The imaginary part of the wave number is a measure of the rate of attenuation with distance within the material, and for the material considered here, it is not very large. In addition, see reference [24] for a discussion of practical matters related to the estimation of the imaginary part of the wave number.

Fig. 12. *Wave number, k_p, for three layers of THL material. Real and imaginary parts of the wave number. Frequency range: 20 Hz – 1.6 kHz. Red curves: Large tube. Blue curves: Small tube*

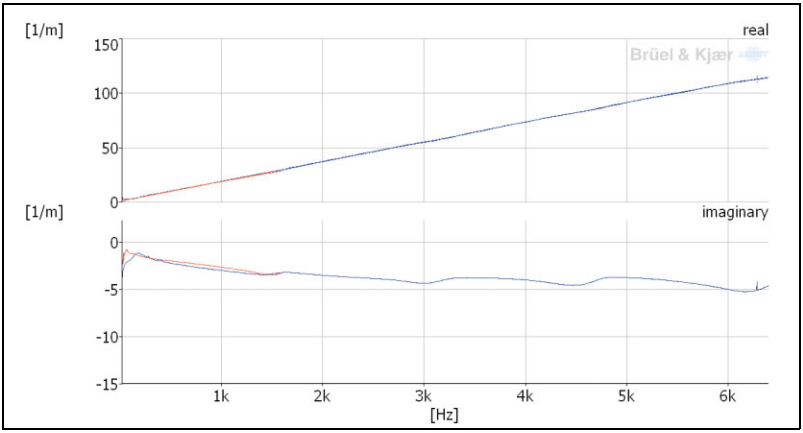

The information represented by the wave number components can be plotted in a more immediately meaningful form. For example, the phase speed in the porous material, c_{ph}, can be expressed in normalised form as:

$$\frac{c_{ph}}{c} = \frac{\omega}{c\mathrm{Re}\{k_p\}} \tag{22}$$

where Re{ } denotes the real part. The normalised phase speeds are plotted in Fig. 14, where it can be seen that the phase speed within the material approaches the ambient sound speed in the high frequency region, but may be significantly less than ambient at low frequencies.

Note that since the phase speed within a porous material is usually reduced compared to that in air, higher order duct modes may "cut on" within the porous material at frequencies lower than they would in air, approximately by the ratio of the phase speeds in the porous material and in the ambient medium. In a dissipative medium there is, of course, no longer a strict distinction between propagating and non-propagating modes and hence no definite cut on frequency. Nevertheless, the existence of higher order modes may affect the accuracy of results at frequencies where higher order modes could propagate in the absence of dissipation.

The acoustical dissipation within a porous material may be expressed in terms of the attenuation per wavelength, which is also plotted in Fig. 15. This quantity is calculated as $-\mathrm{Im}\{k_p\}\ \lambda_p$ where Im{ } denotes the imaginary part, and $\lambda_p = f/c_{ph}$ (where f is the frequency) is the wavelength within the material. The attenuation per wavelength may thus be calculated as: $-2\pi \mathrm{Im}\{k_p\}/\mathrm{Re}\{k_p\}$.

It may be seen that the attenuation per wavelength decreases with frequency owing to the relatively low flow resistivity of the THL.

The characteristic impedance of the THL material is shown in Fig. 13, where it may be seen that the real part of the normalised characteristic impedance is only slightly greater than unity and that the imaginary part is only slightly less than zero. That is, the material's characteristic impedance is very close to that of ambient air, with the result that sound transmits into this material very easily.

Fig. 13. *Normalised characteristic impedance for three layers of THL material.* ***(a):*** *Frequency range: 50 Hz – 1.6 kHz,* ***(b):*** *Frequency range: 50 Hz – 6.4 kHz*

13a.

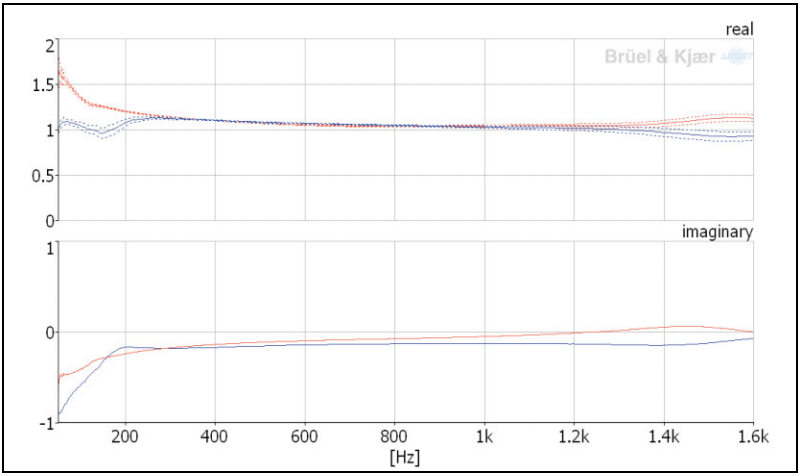

13b.

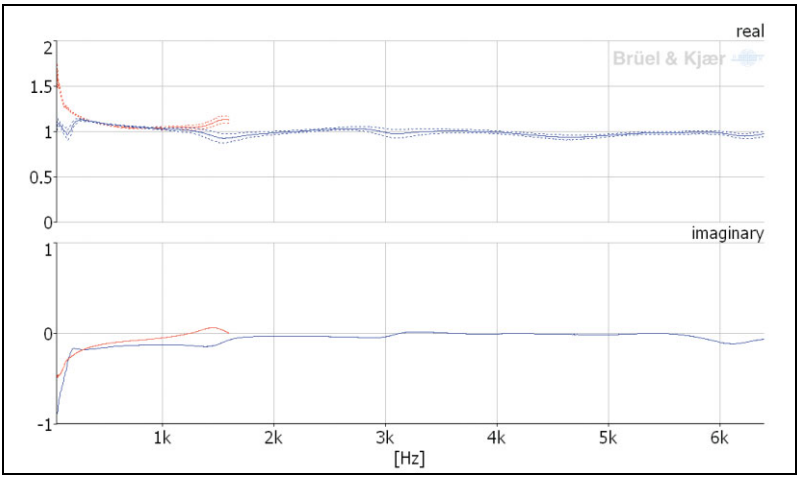

Fig. 14. *Normalised phase speed, c_{ph}/c, per wavelength. Red curves: Large tube. Blue curves: Small tube.* ***(a):*** *Frequency range: 20 Hz – 1.6 kHz,* ***(b):*** *Frequency range: 20 Hz – 6.4 kHz*

14a.

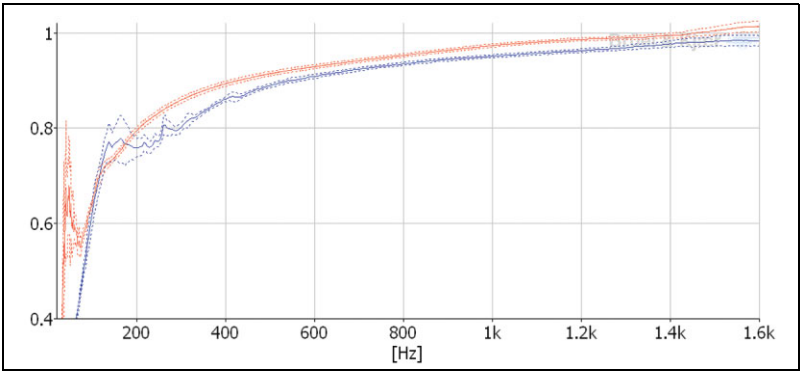

14b.

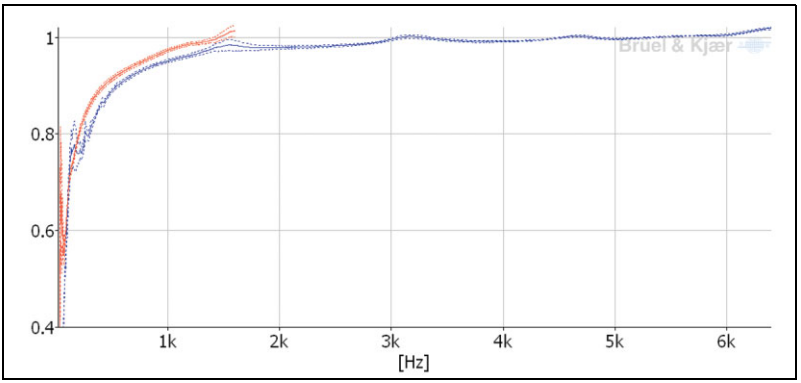

Fig. 15. *Attenuation per wavelength. Red curves: Large tube. Blue curves: Small tube.* ***(a):*** *Frequency range: 20 Hz – 1.6 kHz,* ***(b):*** *Frequency range: 20 Hz – 6.4 kHz*

15a.

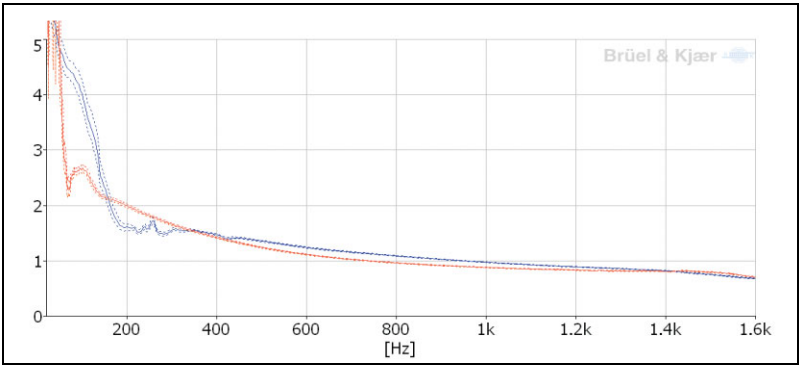

15b.

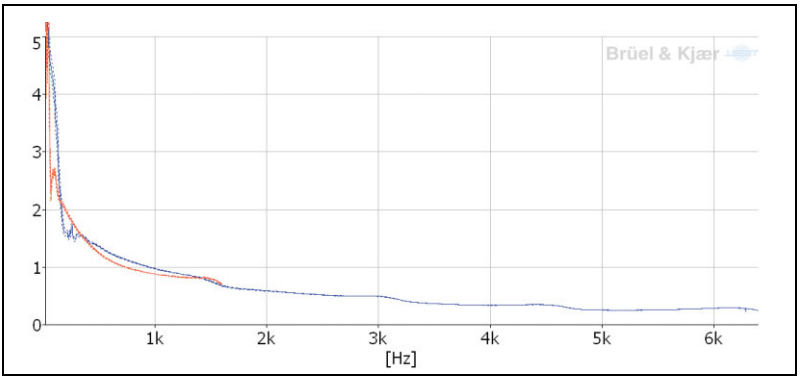

It should be emphasised in closing this sub-section that elastic porous materials such as foams can support two longitudinal waves and a single transverse wave.[38,39] Although a single airborne wave is often dominant in unfaced noise control foams, in which case they can be modeled as effective fluids (see reference [21], for example), the other two wave types may sometimes contribute very significantly, depending on the details of the foams' surface boundary conditions.[39] When the latter is the case, it is no longer possible to specify a material's properties in terms of a single characteristic impedance and wave number. Thus, a transfer matrix representation of a foam layer is, in principle, much more complicated than that presented here as Eq. (16).[13,23] The reader should, therefore, be cautious when applying the present

method for determining characteristic impedance and wave number (and the related properties considered in the next sub-section) to foams.

E. Complex Density and Sound Speed

As mentioned in the last sub-section, homogeneous and isotropic limp or rigid porous materials may be modeled as fluids having complex properties. Thus, arbitrarily-shaped porous material domains may be modeled by using existing finite and boundary element codes so long as provision has been made for complex material properties. The input data most often required by these programs are complex density and the complex sound speed within the porous material. The complex density can be calculated in normalised form as:

$$\frac{\rho_p}{\rho_0} = \frac{(\rho_p c_p) k_p}{\rho_0 \omega} \tag{23}$$

and the normalised complex sound speed as:

$$\frac{c_p}{c} = \frac{\omega}{k_p c} \tag{24}$$

The normalised complex density of the present material is shown in Fig. 16 where it can be seen that the real part is very close to the ambient density of air (approximately 1.2 kg/m^3) and that the imaginary part asymptotes towards zero at high frequencies. Note that the complex density used here is a bulk density in contrast to the pore-based complex density referred to in reference [23]. The two quantities differ by a factor of porosity.

The complex sound speed is shown in Fig. 17. It can be seen that the real part approaches the ambient sound speed at high frequencies and that the imaginary part asymptotes towards zero at the same time, since the dissipation per wavelength within the material decreases with increasing frequency in this case. It should be noted that the phase speed and the real part of the complex sound speed are not the same in general, although for this material they are very close to one another.

Fig. 16. *Normalised complex density, ρ_p/ρ_0, for three layers of THL material. Red curves: Large tube. Blue curves: Small tube.* ***(a):*** *Frequency range: 50 Hz – 1.6 kHz,* ***(b):*** *Frequency range: 50 Hz – 6.4 kHz*

16a.

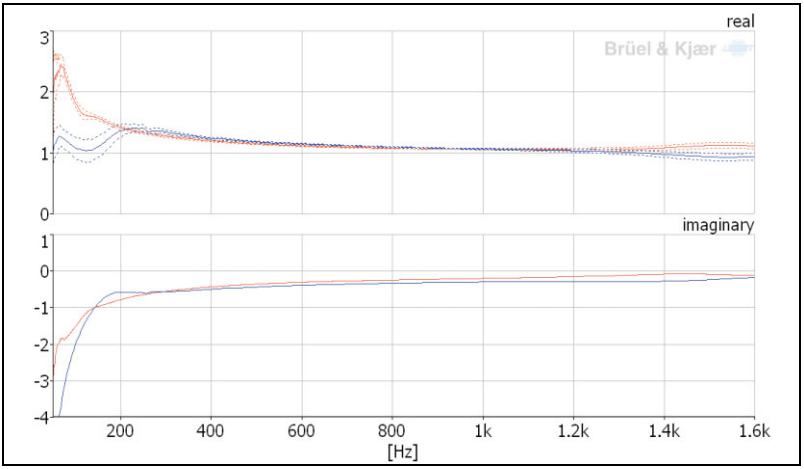

16b.

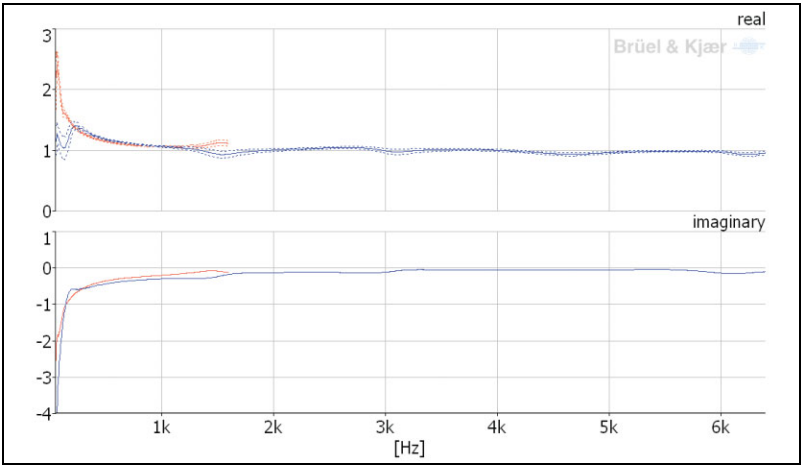

Fig. 17. *Normalised complex sound speed, c_p/c, for three layers of THL material. Red curves: Large tube. Blue curves: Small tube.* ***(a):*** *Frequency range: 20 Hz – 1.6 kHz,* ***(b):*** *Frequency range: 20 Hz – 6.4 kHz*

17a.

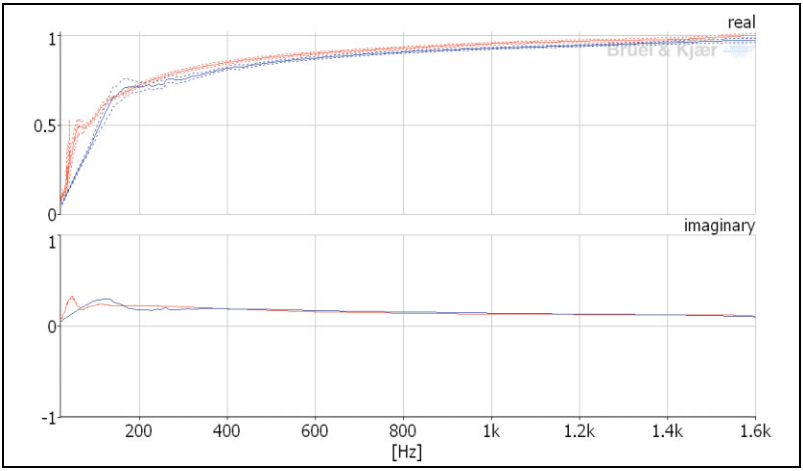

17b.

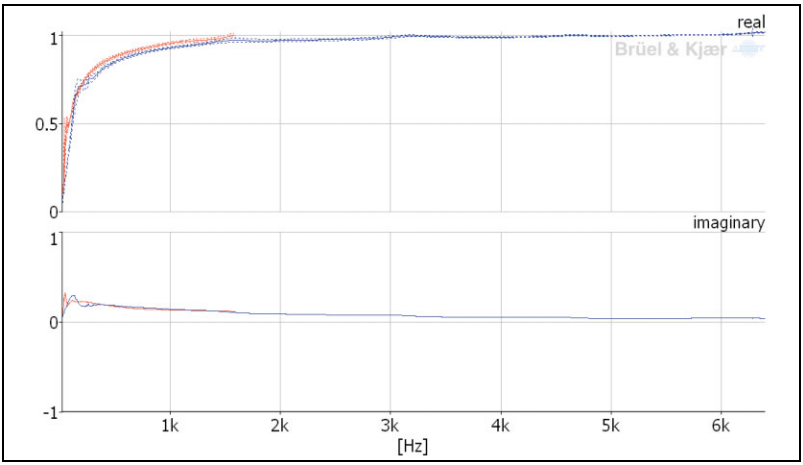

Conclusions

In the present article, we have described a quick and convenient method for determining the normal incidence acoustical properties of samples placed in a standing wave tube. The procedure is based on well-known transfer matrix methods, but has here been adapted to the identification of the properties of acoustical materials. Both one- and two-load implementations of the transfer matrix method have been described, and the conditions under which the one-load method may be used have been specified. The practical use of the transfer matrix procedure has been illustrated by performing measurements on a fibrous material. The transmission losses at various densities of this material were presented along with associated absorption coefficients and surface impedances. Further, it was shown that for porous materials that can be modeled as effective fluids, the characteristic impedance and wave number within the sample can be determined along with the material's complex density and sound speed. The latter information can be used to model limp or rigid porous materials in existing finite element procedures, thus the present procedure may prove a useful adjunct to modern noise control design procedures.

Acknowledgments

The first author is grateful to Joe Pope (formerly of Bruel & Kjaer), who first suggested the use of a four-microphone method to measure the transmission loss of porous materials; to David Apfel of L & L Products of Romeo, Michigan, whose initial financial support helped make the development of the current procedure possible; and, to Robert Schlinker of the United Technologies Research Center, who arranged for additional financial support. Thanks also to Bruel & Kjaer for providing the measurement equipment used in the present work, and to Jonathan H. Alexander of 3M Corporation, who provided acoustical materials for testing purposes.

References

[1] J.S. Bolton, R.J. Yun, J. Pope, and D. Apfel, "*Development of a new sound transmission test for automotive sealant materials*", SAE Trans., J. Pass. Cars 106, pp. 2651 – 2658 (1997).

[2] K. Attenborough, "*Acoustical characteristics of porous materials*", Phys. Rep. 82, pp. 179 – 227 (1982)

[3] H.Y. Lai, S. Katragadda, J.S. Bolton and J.H. Alexander, "*Layered fibrous treatments for sound absorption and transmission*", SAE Trans., J. Pass. Cars 106, pp. 3311 – 3318 (1997).

[4] D.N. Johnston, D.K. Longmore and J.E. Drew, "*A technique for the measurement of the transfer matrix characteristics of two-port hydraulic components*", Fluid Power Sys. and Tech. 1, pp. 25 – 33 (1994).

[5] C. Bordone-Sacerdote and G.G. Sacerdote, "*A method for measuring the acoustic impedance of porous materials*", Acustica 34, pp. 77 – 80 (1975).

[6] M. Fukuda, "*A study on the exhaust muffler of internal combustion engine*", Bull. JSME 6, No. 22, pp. 255 – 269 (1963).

[7] T.Y. Lung and A.G. Doige, "*A time-averaging transient testing method for acoustic properties of piping systems and mufflers with flow*", J. Acoust. Soc. Am. 73, pp. 867 – 876 (1983).

[8] M.L. Munjal, *Acoustics of Ducts and Mufflers* (John Wiley and Sons, New York, NY, 1987).

[9] A.G. Doige, M.L. Munjal and H.S. Alves, "*An improved experimental method for determining transfer matrices of pipeline elements with flow*", Proceedings from NOISE-CON 1988, pp. 481 – 486 (Noise Control Foundation, Poughkeepsie, NY, 1988).

[10] M.L. Munjal and A.G. Doige, "*Theory of two source-location method for direct experimental evaluation of the four-pole parameters of an aeroacoustic element*", J. Sound Vib. 141, pp. 323 – 333 (1990).

[11] K.S. Peat, "*A transfer matrix for an absorption silencer element*", J. Sound Vib. 146, pp. 353 – 360 (1991).

[12] K.U. Ingard and T.A. Dear, "*Measurement of acoustic flow resistance*", J. Sound Vib. 103, pp. 567 – 572 (1985).

[13] K.U. Ingard, *Notes on Sound Absorption Technology* (Noise Control Foundation, Poughkeepsie, NY, 1994).

[14] J.D. McIntosh, M.T. Zuroski and R.F. Lambert, "*Standing wave apparatus for measuring fundamental properties of acoustic materials in air*", J. Acoust. Soc. Am. 88, pp. 1929 – 1938 (1990).

[15] Y. Champoux and M.R. Stinson, "*Measurement of the characteristic impedance and propagation constant of materials having high flow resistivity*", J. Acoust. Soc. Am. 90, pp. 2182 – 2191 (1991).

[16] T. Iwase, Y. Izumi and R. Kawabata, "*A new measuring method for sound propagation constant by using sound tube without any air spaces back of a test material*", Proc. INTER-NOISE 1998, 4 pages (CD-ROM edition, Causal Productions, Australia, 1998).

[17] P. Dean, "*An in situ method of wall acoustic impedance measurement in flow ducts*," J. Sound Vib. 34, 97 – 130 (1974).

[18] C.K. Amedin, Y. Champoux and A. Berry, "*Acoustical characterization of absorbing porous materials through transmission measurements in a free field*", J. Acoust. Soc. Am. 102, pp. 1982 – 1994 (1997).

[19] B.H. Song and J.S. Bolton, "*A transfer matrix approach for estimating the characteristic impedance and wave numbers of limp and rigid porous materials*", J. Acoust. Soc. Am. 107, pp. 1131 – 1152 (2000).

[20] A.D. Pierce, Acoustics: An Introduction to its Physical Principles and Applications (McGraw-Hill, New York, NY, 1981).

[21] A.F. Seybert, R.A. Seman and M.D. Lattuca, "*Boundary element prediction of sound propagation in ducts containing bulk absorbing materials*", Trans. ASME, J. Vib. and Acoust. 120, pp. 976 – 981 (1998).

[22] S. Temkin, Elements of Acoustics (Wiley, New York, 1981).

[23] J.F. Allard, Propagation of Sound in Porous Media (Elsevier Applied Science, London and New York, 1993).

[24] J. Huebelt, M. Boehm and R. Hoffmann, "*Using an extended impedance measurement method for the estimation of porosity and flow resistance of porous materials*", Proc. Twelfth International Congress on Sound and Vibration, (2005).

[25] A.F. Seybert and J.F. Hamilton, "*Time-delay bias errors in estimating frequency response and coherence functions*", Journal of Sound and Vibration 60, pp. 1 – 9 (1978).

[26] M.S. Kompella, P. Davies, R.J. Bernhard and D.A. Ufford, "*A technique to determine the number of incoherent sources contributing to the response of a system*", Mechanical Systems and Signal Processing 8, pp. 363 – 380 (1994).

[27] J. Kruger and M. Quickent, "*Determination of acoustic absorber parameters in impedance tube*", Ap. Acoust. 50, pp. 79 – 89 (1997).

[28] Seung-Ho Jang and Jeong-Guon Ih, "*On the multiple microphone method for measuring in-duct acoustic properties in the presence of mean flow*", J. Acoust. Soc. Am. 103, pp. 1520 – 1526 (1998).

[29] Anon., "*Standard test method for impedance and absorption of acoustical materials using a tube, two microphones, and a digital frequency analysis system*", ASTM Standard E 1050-98(1990).

[30] L.L. Beranek, "*Some notes on the measurement of acoustic impedance*", J. Acoust. Soc. Am. 19, pp. 420 – 427 (1947).

[31] B.H. Song, J.S. Bolton and Y.J. Kang, "*Effect of circumferential edge constraint on the acoustical properties of glass fiber materials*", J. Acoust. Soc. Am. 110, pp. 2902 – 2916 (2001)

[32] B.H. Song and J.S. Bolton, "*Investigation of the vibrational modes of edge-constrained fibrous samples placed in a standing wave tube*", J. Acoust. Soc. Am. 113, pp. 1833 – 1849 (2003)

[33] Y.J. Kang and J.S. Bolton, "*A finite element model for sound transmission through foam-lined double panel structures*", J. Acoust. Soc. Am. 99, pp. 2755 – 2765 (1996).

[34] Y.J. Kang and J.S. Bolton, "*Sound transmission through elastic porous wedges and foam layers having spatially graded properties*", J. Acoust. Soc. Am. 102, pp. 3319 – 3332 (1997).

[35] Anon., "*Standard test method for the laboratory measurement of airborne sound transmission loss of building partitions and elements*", ASTM Standard E 90-02(2002).

[36] T. Yoo, J. S. Bolton and J. H. Alexander, "*Prediction of random incidence transmission loss based on normal incidence four-microphone measurements*", Proc. INTER-NOISE 2005 (2005)

[37] B.A. Biot, "*Theory of propagation of elastic waves in a fluid-saturated porous solid*", J. Acoustics. Soc. Am. 28, pp. 168 – 191 (1956).

[38] J.S. Bolton and Y.J. Kang, "*Elastic porous materials for sound absorption and transmission control*", SAE Trans., J. Pass. Car 106, pp. 2576-2591 (1997).

[39] J.S. Bolton, N.M. Shiau, and Y.J. Kang, "*Sound transmission through multi-panel structures lined with elastic porous materials*", J. Sound Vib. 191, pp. 317 – 347 (1996).

Previously issued numbers of Brüel & Kjær Technical Review

(Continued from cover page 2)

2 – 1994 The use of Impulse Response Function for Modal Parameter Estimation
Complex Modulus and Damping Measurements using Resonant and Non-resonant Methods (Damping Part II)
1 – 1994 Digital Filter Techniques vs. FFT Techniques for Damping Measurements (Damping Part I)
2 – 1990 Optical Filters and their Use with the Type 1302 & Type 1306 Photoacoustic Gas Monitors
1 – 1990 The Brüel & Kjær Photoacoustic Transducer System and its Physical Properties
2 – 1989 STSF — Practical Instrumentation and Application
Digital Filter Analysis: Real-time and Non Real-time Performance
1 – 1989 STSF — A Unique Technique for Scan Based Near-Field Acoustic Holography Without Restrictions on Coherence
2 – 1988 Quantifying Draught Risk
1 – 1988 Using Experimental Modal Analysis to Simulate Structural Dynamic Modifications
Use of Operational Deflection Shapes for Noise Control of Discrete Tones
4 – 1987 Windows to FFT Analysis (Part II)
Acoustic Calibrator for Intensity Measurement Systems
3 – 1987 Windows to FFT Analysis (Part I)
2 – 1987 Recent Developments in Accelerometer Design
Trends in Accelerometer Calibration
1 – 1987 Vibration Monitoring of Machines

Special technical literature

Brüel & Kjær publishes a variety of technical literature which can be obtained from your local Brüel & Kjær representative.
The following literature is presently available:

- Catalogues (several languages)
- Product Data Sheets (English, German, French,)

Furthermore, back copies of the Technical Review can be supplied as listed above. Older issues may be obtained provided they are still in stock.

BV 0059– 11 ISSN 0007–2621

HEADQUARTERS: DK-2850 Nærum · Denmark
Telephone: +45 45 80 05 00 · Fax: +45 45 80 14 05
www.bksv.com · info@bksv.com

Brüel & Kjær